Heliyon 11 (2025) e41935

Contents lists available at ScienceDirect

Heliyon

journal homepage: www.cell.com/heliyon

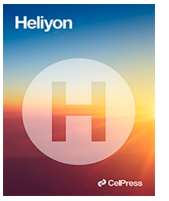

Research article

ISCOM-type matrix from beta-escin and glycyrrhizin saponins

V. Petkov [a], S. Tsibranska [a], I. Manoylov [b], L. Kechidzhieva [b], K. Ilieva [b], S. Bradyanova [b], N. Ralchev [b], N. Mihaylova [b], N. Denkov [a], A. Tchorbanov [b,**], S. Tcholakova [a,*]

[a] Department of Chemical Engineering, Sofia University, Sofia, Bulgaria
[b] Department of Immunology, Institute of Microbiology, Bulgarian Academy of Sciences, Sofia, Bulgaria

ARTICLE INFO

Keywords:
Nanoparticles
Toxicity
Liposomes
Immune targeting device

ABSTRACT

Background and aims: Nanotechnology provides the opportunity for construction of modern transport devices such as nanoparticles for a variety of applications in the field of medicine. A novel experimental protocol for the formation of saponin-cholesterol-phospholipid nanoparticles of vesicular structure has been developed and applied to prepare stable nanoparticles using escin or glycyrrhizin as saponins.

Methods: The methods for nanoparticle construction include a sonication at 90 °C of the initial mixture of components, followed by an additional sonication on the next day for incorporation of an additional amount of cholesterol, thus forming stable unilamellar vesicles. Tests and assays for cell viability, erythrocyte hemolysis, flow cytometry, and fluorescent microscopy analyses have been performed.

Results: By selecting appropriate component ratios, stable and safe particles were formulated with respect to the tested bio-cells. The prepared nanoparticles have mean diameter between 70 and 130 nm, depending on their composition. The versatility of these nanoparticles allows for the encapsulation of various molecules, either within the vesicle interior for water-soluble components or within the vesicle walls for hydrophobic components. The saponin particles formed after cholesterol post-addition (E3-M2) are stable and 100 % of the cells remain viable even after 10-times dilution of the initial particle suspension. These particles are successful included into isolated mouse macrophages.

Conclusions: Among the variety of generated nanoparticles, the E3-M2 particles demonstrated properties of safe and efficient devices for future vaccine design and antigen targeting to immune system.

1. Introduction

Adjuvants are substances used to enhance the immune response, and to reduce the amount of antigen in the vaccine formulation and number of immunizations needed to develop protection against a certain pathogen. The immunostimulating complex (ISCOM) was

* Corresponding author. Department of Chemical and Pharmaceutical Engineering Faculty of Chemistry and Pharmacy, Sofia University 1 James Bourchier Ave., 1164, Sofia, Bulgaria.
** Corresponding author. Department of Immunology, Institute of microbiology, Bulgarian Academy of Science 26 Georgi Bonchev str., 1113, Sofia, Bulgaria.
E-mail addresses: tchorban@microbio.bas.bg (A. Tchorbanov), SC@LCPE.UNI-SOFIA.BG (S. Tcholakova).

https://doi.org/10.1016/j.heliyon.2025.e41935
Received 19 February 2024; Received in revised form 12 January 2025; Accepted 12 January 2025
Available online 13 January 2025

described in the literature 40 years ago by Morein et al. [1]. ISCOM's are nanoparticles composed of cholesterol, saponin (usually the natural extract from the bark of the *Quillaja Saponaria*, Quil A), phospholipids and respective antigen [2–4]. ISCOM matrix (i.e. ISCOM without added antigen) [4,5] contains cholesterol (denoted as "chol"), Quil A and phospholipids (PCs) which self-assemble into a cage-like structure. The matrix allows encapsulation of different antigens such as para-influenza-3 (PI-3) [1]; herpes simplex virus type 2 (HSV-2) [6]; human immunodeficiency virus (HIV) [7], Newcastle disease [8], etc. Recently, Novavax has developed an adjuvanted vaccine targeting the SARS-CoV-2 spike protein, NVX-CoV2373 (Nuvaxovid™), which has efficacy for the prevention of COVID-19 [9–11]. This vaccine used Matrix-M adjuvant [12], consisting of two different forms of ISCOM nanoparticles prepared by two different fractions of *Quillaja Saponaria*, namely Quil A and Quil C [13–15].

Several methods for ISCOM matrix preparation are described in the literature. The traditional methods include the usage of surfactants for solubilization of cholesterol and phospholipids [1]. In the centrifugation method, the replacement of surfactant (usually Triton X 100) occurs during centrifugation through a sucrose gradient [16]. The method is relatively simple, but the amount of formed ISCOMs matrices is unsatisfactory [17]. In the dialysis method, the surfactant (usually Mega 10) is used to solubilize cholesterol, phospholipids and Quil A, and it is removed afterwards by dialysis for at least 3 days [18–23]. Pham et al. developed a surfactant-free method for preparation of ISCOMs [17]. In this method, instead of surfactant, an ether was used for dissolution of cholesterol and phospholipids. The ether solution was mixed with Quil A containing aqueous solution with the optimal ratio for ISCOMs preparation PC:Quil A:Chol 5:3:2 [17]. This method has been used for preparation of saponinosomes from Ziziphus spina-christi as a cancer drug carrier [24]. Instead of ether, Lendemans et al. [25] proposed the usage of ethanol for dissolution of cholesterol and phospholipids before they were mixed with aqueous solution of Quil A. The method is relatively fast (2 h), and saponin from Carica papaya leaves has been used for preparation of the ISCOM matrix [26]. In the lipid film hydration method, a thin layer of dried cholesterol and phospholipids is placed in contact with a Quil A solution [27]. Then the solution is stirred, which leads to swelling of the layer and spontaneous formation of liposomes. This method is simple (PC:Quil A:Chol ratio is 6:4:1), but the obtained particles are more heterogeneous as compared to those, prepared by the dialysis method [28,29]. In the reverse phase evaporation method [30], the lipids are dissolved in a mixture of solvents, which leads to the formation of inverted micelles. The aqueous phase is added, resulting in the formation of a water-in-oil emulsion, which is emulsified by stirring or sonication. The removal of the solvent is achieved by rotary evaporation, which leads to the formation of a gel phase that finally collapses to form liposomes [30]. In all methods described in the literature [30], surfactants or solvents are used during the preparation procedure and must be removed afterwards. In the experimental protocol proposed in the current study, neither surfactant nor solvent is used.

Escin is a triterpenoid saponin that exhibits anti-inflammatory and antiedema effects [31]. Formation of novel structures in a mixture of β-escin, dipalmitoylphosphatidylcholine (DPPPC) and cholesterol with a size of 100–200 nm was reported previously [32]. However, their adjuvant and hemolytic effects have not been studied so far.

The glycyrrhizin is the main active compound in licorice. Its antiviral [33] and immune stimulant activities against duck hepatitis virus [34], as well as an adjuvant effect on the efficacy of lactococcosis vaccine in rainbow trout (*Oncorhynchus mykiss*) has been shown in Ref. [35]. The glycyrrhizin also prevents hemorrhagic transformation and improves neurological outcome in ischemic stroke with delayed thrombolysis [36]. The incorporation of glycyrrhetinic acid in liposomes further enhances the immune response against Newcastle disease vaccine compared with the adjuvant alone [37]. Luo et al. discussed the therapeutic potential of glycyrrhizin for the treatment of COVID-19 [38]. Bailly & Vergoten also proposed the usage of glycyrrhizin for therapy of the same disease, because it is considered as a safe natural product, with a long-tested use in humans as a hepatoprotective agent [39]. Glycyrrhizin has been also used for the treatment of chronic hepatitis (and other liver diseases) and has been proven to act against some coronaviruses such as the porcine virus (PEDV). Furthermore, it has been shown that glycyrrhizin exhibits promising outcomes against SARS-CoV-2. Diammonium glycyrrhizinate in combination with vitamin C has been tested in clinical trials for COVID-19 treatment [40].

The functional property of many nanoparticles (NP) is the delivery of anti-cancer drugs and different cell-death applications [41]. In contrast, ISCOMs are primarily used for vaccine elements delivery and immunotherapy. However, ISCOMS's cytotoxicity is the main limitation factor for their exploration and exploitation [42–45]. Therefore, during the generation of these nanoparticles, their toxicity, together with the immunostimulating effect, will be evaluated.

The aim of the current study is to develop a fast solvent-free and surfactant-free method for preparation of ISCOM matrix particles which can be easily utilized for preparation of nanoparticles from different saponins. To the best of our knowledge, this study is the first to propose the formation of nanoparticles using the saponins escin and glycyrrhetinic acid, rather than Quil A. These two saponins could have very different adjuvant effects compared to the traditionally used Quil A. Utilizing escin and glycyrrhetinic acid for nanoparticles creation is beneficial, as these saponins are extracted from trees native to Europe, whereas Quil A is derived from *Quillaja saponaria Molina* which is commonly found only in South America. The safety of these particles is tested together with their ability to be internalized by phagocytic cells *in vitro*, based on defined protocols for the initial stages of the pre-clinical trials for vaccine development [46,47]. After safety and functional validation, these ISCOMs will be used for the generation of a COVID-19 vaccine and tested *in vivo*.

2. Materials and methods

2.1. Materials

For preparation of the ISCOM matrix we used triterpenoid monodesmosidic saponins: β-escin purchased from Sigma-Aldrich (Taufkirchen, Germany; purity ≥95 %; cat. No E1378-10G) and licorice - glycyrrhizic acid (ammonium salt) extracted from glycyrrhiza root, product of Sigma-Aldrich (purity ≥95 %; cat. No 50531-50G). Cholesterol was purchased from Sigma-Aldrich (purity ≥95

%; cat. no. 26740); 1,2-dipalmitoyl-sn-glycero-3-phosphocholine (DPPC) was obtained from Coatsome (NOF American corporation, White Plains, NY) (MC-6060). For buffers and solutions preparation, we used NaCl and KCl purchased from Sigma-Aldrich; Na_2HPO_4 from Carlo Erba (Emmendingen, Germany, 480 144) and KH_2PO_4 from Fluka (Buchs, Switzerland, 60 220-1 KG). For gas chromatography (GC) and high performance liquid chromatography (HPLC) analyses we used N,O-Bis(trimethylsilyl)trifluoroacetamide (BSTFA, Sigma, T6381-10G), pyridine with purity of 99.8 % (Sigma, 270 970-100 ML), chloroform with purity of 99.98 % (Honeywell, Morris Plains, New Jersey, 319 988), and hexadecanol with purity of 99 % (Sigma, C-7882). All aqueous solutions were prepared with deionized water from water-purification system Elix 3 RiOs (Millipore, Burlington, MA).

2.2. ISCOM's preparation protocol

All samples were prepared in a phosphate-buffered saline (PBS) buffer (containing 137 mM NaCl, 2.7 mM KCl, 8.1 mM Na_2HPO_4, and 1.76 mM KH_2PO_4). The required amount of saponin was dissolved in 10 ml PBS, followed by the addition of DPPC and cholesterol. The samples were heated up to 90 °C and homogenized with a pulse sonicator (SKL-650W, Syclon, Ningbo Haishu Sklon Electronic Instruments Co, Zhejiang, China) in a series of 1 s long pulses at 500W with 1 s power off. The total time for each sonication cycle was 10 min (including power on and power off periods). The temperature during sonication was maintained at 90 °C by water bath. After each sonication cycle, the sample was stored at 90 °C for 10 min before the next sonication cycle started. Each sample underwent a total of 3 sonication cycles during preparation. Afterwards, the samples were stored overnight at room temperature. The composition of prepared samples is shown in Table 1 below.

The following day, 4.5 mg of cholesterol were added to certain samples, and 7 additional sonication cycles were applied to obtain stable nanoparticles with low hemolytic activity. These samples are denoted as modified samples in the text below.

In some cases, Nile Red or Bodipy (1 mM) fluorescent dyes were included as described in section 2.8 below.

2.3. Turbidity measurements

The turbidity measurements were performed using Jasco Spectrophotometer V-730 (Easton, MD) at a wavelength of 500 nm at 20 °C temperature.

2.4. Centrifugation

The samples were centrifuged for 1 h at 20 000 g (5000 rpm) on SIGMA 3-16 PK centrifuge (Sigma Laborzentrifugen GmbH, Osterode am Harz, Germany) to obtain a clear aqueous phase (serum) and sediment. Finally, the serum was filtered through a 200 nm syringe filter (Sartorius, Goettingen, Germany) to obtain the suspension of ISCOM particles for further investigations.

Table 1
Composition of prepared samples, their absorbance measured before centrifugation and filtration, mean sizes (by volume, intensity and number), and PDI determined for centrifuged and filtered samples.

	ESC	CH	DPPC	Absorbance	z_{ave}, nm	PDI	d_v, nm	d_I, nm	d_N, nm
E1	10	10	80	2.70	92	0.23	55	124	30
	30	10	60	2.34	141	0.29	92	229	24
E2									
	50	10	40	0.65	93	0.18	83	115	57
E3									
	20	20	60	3.08	126	0.12	124	144	86
E4									
	30	25	45	2.95	115	0.04	110	122	92
E6									
	10	35	55	2.88	101	0.16	87	121	57
E8									
	20	40	40	2.75	91	0.13	78	102	60
E9									
	30	40	30	2.85	129	0.34	530	399	63
E11									
	40	20	40	2.39	128	0.14	126	151	81
E15									
	60	10	30	0.59	80	0.15	68	95	50
E16									
	40	10	50	0.88	100	0.24	96	133	59
E17									
	47.5	5	47.5	0.32	69	0.26	18	91	12
E20									

ESC = escin; CH = cholesterol; DPPC = 1,2-dipalmitoyl-sn-glycero-3-phosphocholine; z_{AVE} = intensity based harmonic mean (2,3); PDI = polydispersity index; d_V = mean volume diameter; d_I = mean diameter by intensity; d_N = mean diameter by number.

2.5. Dynamical light scattering (DLS)

DLS was performed using the Zetasizer Nano ZS instrument (Malvern Instruments, Malvern, UK). All measurements were conducted at 25 °C. Solid-state laser with wavelength of 633 nm was used as a light source and the experiments were performed at 173° scattering angle. From the measured autocorrelation function of the scattered light, the instrument calculates particle size characteristics: Z-ave which is intensity based harmonic mean (2,3), polydispersity index (PDI), and the mean sizes by volume (d_V), by intensity (d_I), and by number (d_N).

2.6. Gas chromatography

The prepared samples were heated to 60 °C and the aqueous phase was allowed to evaporate at this temperature. Then, the solid residue was dissolved in 400 μL chloroform which contained an internal standard (hexadecanol), followed by addition of 200 μL pyridine and BSTFA. Following the derivatisation process, which lasted 60 min at 60 °C, the samples were diluted with iso-octane and analyzed by GC. The cholesterol content was analyzed on Agilent 8890 (Agilent technologies, Santa Clara, CA) connected to autosampler 7693A. Agilent DB-5HT capillary column with the following specifications was used: (5%-Phenyl)-methylpolysiloxane, 30 m length, I.D. 0.32 mm, 0.1 μm film thickness. An injection volume of 1 μL and cold on-column injection was used. The oven was programmed in the following way: start at 60 °C, hold 1 min, the 1st ramp is up to 180 °C at 10 °C/min, hold 0 min, 2nd ramp is to 375 °C at 30 °C/min, hold 10 min. Sample analysis time was 29.5 min. The flame ionization detector was operated at T = 380 °C. Helium at a constant flow rate of 2 mL/min was used as a carrier gas. Hydrogen, air, and nitrogen (make-up gas) were used as detector gasses. The concentrations of cholesterol were calculated from the internal standard hexadecanol.

2.7. Cryogenic transmission electron microscopy (cryo-TEM)

The ISCOM nanoparticles were observed using cryo-TEM. Vitrobot system (FEI, USA) was used for specimen preparation at 25 °C and 100 % relative humidity. Briefly, a drop of the tested dispersion sample was placed on a holey carbon copper TEM grid, the excess liquid was blotted off with filter paper, and then the sample was plunged into a liquid propane-ethane mixture to form a vitrified specimen. Afterwards, the specimen was transferred into a liquid nitrogen and stored until further inspection. The cryo-TEM imaging was performed using the Gatan cryo-specimen holder at JEM-2100 (JEOL, Tokyo, Japan) high-resolution transmission electron microscope. An acceleration voltage of 200 KeV was used, and the micrographs were recorded with a Gatan Orius SC1000 camera.

2.8. Incorporation of the fluorescent dyes Nile Red and Bodipy into the particles

Fluorescent dyes were incorporated in the particles in concentration 1 mM. The incorporation was done by adding the dye to the saponin solution together with the cholesterol and the DPPC. The samples were heated up to 90 °C and homogenized with a pulse sonicator in a series of 1 s long pulses at 500W with 1 s power off and following the protocol described in *section 2.2*.

2.9. Cell cultures

A20 cell line derived from mouse reticulum cell sarcoma (TIB-208) (RRID: CVCL_1940) and CT26.WT cell line derived from mouse colon adenocarcinoma (CRL-2638) (RRID: CVCL_7256) were purchased from American Tissue Culture Collection, ATCC (Manassas, VA, USA). Both cell lines were cultured in Roswell Park Memorial Institute (RPMI) - 1640 medium (R7755, Sigma-Aldrich), supplemented with 10 % heat-inactivated Fetal Bovine Serum (FBS) (F7524, Sigma–Aldrich) and antibiotic/antimycotic solution (A5955, Sigma–Aldrich). The cell cultures were maintained at 37 °C/5 % CO_2 and humidified atmosphere. At the beginning of each experiment, the cell's viability was assessed by Trypan blue exclusion. Cells with viability above 80 % were used in the following experiments. Authentication included STR profiling to confirm genetic identity, morphological evaluation to verify cell characteristics, and growth pattern assessment to match documented profiles. All cell lines utilized in the experiments reported in this study were confirmed to be free of mycoplasma contamination through negative testing.

2.10. Viability assay

To evaluate the effect of the different nanoparticles on the test cells, MTT viability assay was performed [48]. A20 and CTC26.WT cells were centrifuged for 10 min at 130×*g*, diluted 100×, and viability assessed by Trypan blue exclusion. The cells were cultured overnight in 96-well cell culture plates (1×10^4 cells/well) in complete RMPI-1640 medium and maintained at 37 °C/5 % CO_2 and humidified atmosphere. Later, the cells were co-cultured in the presence of serial dilutions of the nanoparticles' solution (10×, 100×, 1000× and 10000×) for 24 h, 48 h and 72 h. Control wells with untreated cells were prepared for each time period. At the end of the experiment, 20 μl of MTT ((3-[4,5-dimethylthiazol-2-yl]-2,5-diphenyltetrazolium bromide; thiazolyl blue, M2128, Sigma-Aldrich) was added (5 mg/ml) into the experimental wells for additional 4 h. The formed formazan crystals were dissolved in 200 μl of dimethyl sulfoxide (DMSO, 276 855, Sigma-Aldrich) and absorbance was measured at 595 nm. The percent of cell viability was calculated using following formula:

$$cells\ viability\ (\%) = \left(\frac{absorbance\ of\ the\ exposed\ cells}{absorbance\ of\ the\ untreated\ cells}\right) x100$$

2.11. Animals

Transgenic 6-week-old B6.Cg-Tg(K18-ACE2)2Prlmn/J mice were purchased from The Jackson Laboratory (Bar Harbor, ME, USA). The animals were housed under specific pathogen free (SPF) conditions in the barrier-type animal house at the Institute of Microbiology with a light/dark cycle of 12/12 h at 20 °C until reaching 10 weeks of age. All manipulations were approved by the Animal Care Commission at the Institute of Microbiology (N286/April 16, 2021) in accordance with the national regulations and the Guidelines for the Care and Use of Laboratory Animals of the European Union (EU Directive 2010/63/EU).

2.12. Experimental design

Untreated 10 weeks old B6.Cg-Tg(K18-ACE2)2Prlmn/J mice (1 group, totally 30 animals) were used as blood donors for erythrocyte hemolysis test as well as for obtaining of mouse peritoneal macrophages. No *in vivo* tests were performed on the animals.

2.13. Blood samples

Blood was obtained from the retro orbital venous sinus, and the blood samples from 12 mice were collected in test tubes, containing 124 mM sodium citrate (Sigma). Centrifugation at 2000×*g* for 5 min was used to separate the erythrocytes from the blood plasma. The enriched fraction was washed 3 times with PBS and finally resuspended in 5 ml PBS.

2.14. Erythrocyte hemolysis

The erythrocyte hemolytic effect of the nanoparticles was assessed using blood samples as 250 μl of the diluted nanoparticles (10×, 100×, 1000× and 10000×) were mixed with 10 μl of the erythrocyte suspension (see above). Control tubes (erythrocytes + PBS and erythrocytes + dH_20) were used to determine the minimal and maximal levels of hemolysis. The tubes were incubated at 37 °C for 1 h on a 3D shaker-incubator at 200 rpm. After the incubation, the samples were centrifuged at 2000×*g* for 5 min and the supernatants (200 μl) were transferred to an ELISA plate. The absorbance was measured at 415 nm using a microplate reader. The percent of erythrocyte hemolysis was calculated using the following formula:

$$erythrocyte\ hemolysis\ (\%) = \left(\frac{absorbance\ of\ the\ experimental\ tubes}{absorbance\ of\ the\ PBS\ tubes}\right) x100$$

2.15. Flow cytometry analysis

To determine whether the produced nanoparticles were interacting with the F4/80 positive macrophages, we used fluorescence-activated cell sorting (FACS). Mouse peritoneal cells were isolated by lavage with PBS, counted and 2×10^5 cells were transferred to FACS tubes. Next, the cells were incubated for 30 min with nanoparticles incorporated with Nile Red, washed, and incubated with anti-F4/80-FITC labeled antibody (123 107, Biolegend) for an additional 30 min. The dye incorporated in nanoparticles was detected by the PE-Texas Red filter, and the percentage of Nile Red-positive F4/80 cells was determined with BD LSR II flow cytometer using the Diva 6.1.1. software (BD Biosciences, Mountain View, CA).

2.16. Fluorescent microscopy analysis

Following the FACS assay, fluorescence microscopy analysis of the cell-included nanoparticles was performed. Peritoneal macrophages isolated as described before were plated on microscope slides (2×10^5 cells per slide) and incubated in Dulbecco's Modified Eagle Medium (DMEM, D5648, Sigma–Aldrich, Merck) supplemented with 10 % heat–inactivated Fetal Bovine Serum (FBS) and antibiotic-antimycotic solution for 24 h at 37 °C/5 % CO2 in humidified atmosphere.

Next, the slides were washed with PBS and were incubated with 10× diluted Nile Red-nanoparticles in complete DMEM medium for another 18 h. Later, the samples were fixed with 4 % Paraformaldehyde (PFA) and permeabilized with 0.2 % Tween-PBS/Ca/Mg. The fixed and permeabilized cells were incubated consecutively with Actin Green 488 ReadyProbes Reagent (AlexaFluor™ 488 phalloidin, R37110, Thermo Fisher Scientific, Waltham, MA) and Hoechst 33 342 Staining Dye Solution (ab228551, Abcam, Cambridge, UK). After 3 washing steps with PBS/Ca/Mg, the slides were mounted and left in the dark to dry. Leica DM6 B microscope (Wetzlar, Germany), and Leica LAS-X software were used for the observation and analysis.

2.17. Statistical analysis

All statistical analyses were performed with Prism software from GraphPad (San Diego, CA). The two-way ANOVA test was used to determine differences between each two groups and values in the figures correspond to mean ± SD. All erythrocyte hemolysis, and viability tests were triplicated. A value of $p < 0.05$ was considered as statistically significant.

3. Results

3.1. Escin particles construction

3.1.1. Particle size and polydispersity of non-modified particles

In the first series of experiments, nanoparticles from escin, DPPC and cholesterol at different ratios were prepared. The turbidity of the initial suspensions after their preparation (before the centrifugation), the sizes, and the PDI of the particles remaining in the solution after centrifugation and filtration, are compared in Table 1. It is seen that most of the samples are very turbid (with absorbance above 1 R.I.), and only samples containing relatively low amounts of cholesterol (≤10 %) and high amounts of escin (≥45 %) are opalescent. After centrifugation and filtration, the samples became transparent and measured z_{ave} values were between 70 and 140 nm, while the mean volume diameter (d_v) varied between 18 nm (sample E20) to 530 nm (sample E11). These results show that a high ratio of saponin to cholesterol is required to obtain clear formulations with particle size suitable for ISCOM development, i.e. between 40 and 80 nm. A fraction of the prepared particles fell within this range. We chose to test the model cell viability after co-incubation with

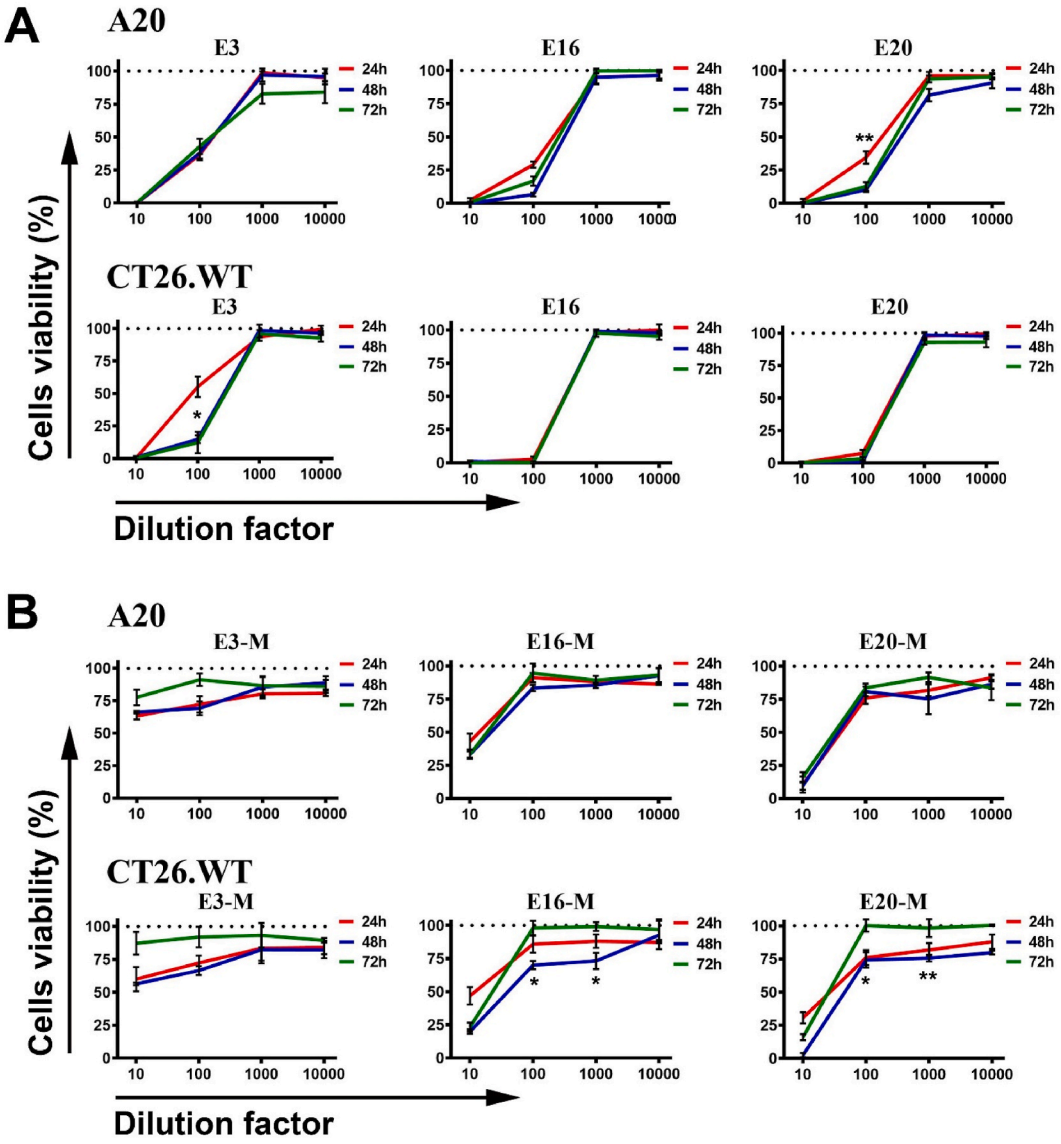

Fig. 1. A20 and CT26.WT cells viability after 24 h (red curves), 48 h (blue curves), and 72 h (green curves) after treatments with particles as a function of dilution. Untreated cells were used as controls with 100 % viability for each time period. **1A.** Treatment of cell lines with samples E3, E16 and E20 from Table 1; **1B.** The same treatment of cell lines with modified particles (samples E3-M, E16-M and E20-M from Table 2). All samples were triplicated and mean ± SD values were presented for each group; p values were calculated using the two-way ANOVA test (*$p < 0.05$; **$p < 0.01$). A representative of three independent experiments is shown.

samples E3, E16, and E20, which had the lowest initial turbidity. This is because, after centrifugation and filtration, a significant fraction of the initially dispersed material was removed from the other samples with higher turbidity. Samples with numbers E5, E7, E10, E12, E13, E14, E18, and E19 contain either very small particles or very large precipitates, which is why they have not been analyzed further.

3.1.2. Cell tests of non-modified particles

The experimental results from the cell tests with the chosen particles, using A20 and CT26 cell lines, showed that the tested cells remain viable after treatment with 1000-folds and 10 000-folds diluted samples, whereas there were practically no viable cells left after treatment with 10-folds diluted samples (Fig. 1A). Significant differences were found comparing the results obtained after 24 h and 72 h incubation using the A20 cell line co-cultured with E20 particles (100×), and when using CT26.WT cells co-cultured with E3 particles (100×). It seems that part of escin molecules were not tightly bound to the particles and remained dissolved as monomers in the aqueous phase.

It is known that β-escin is a surface-active compound which possesses hemolytic potential. The free escin molecules can penetrate the cell membrane and to disrupt its integrity, leading to cell death. The main function of cholesterol in ISCOM particles is to prevent the leakage of free saponin molecules. Better results were achieved with sample E3 at 100-folds dilution, as compared to the results obtained with samples E16 and E20.

3.1.3. Particle size, cell tests and cryo-TEM of modified particles

To decrease the concentration of free escin molecules in the samples, we modified the particle preparation procedure by adding an additional amount of cholesterol to the particles already formed from samples

E3, E16, and E20. An additional 22.5 mg of cholesterol was introduced to these samples through application of 4 extra sonication cycles. The properties of the modified particles are compared with the properties of the initial particles in Table 2. The addition of cholesterol led to significant increase of the samples turbidity and to increase in the mean size of the particles, observed after centrifugation and filtration.

The experimental data from the viability tests on A20 and CT26.WT cells, incubated with modified particles, is shown in Fig. 1B. The addition of cholesterol to all studied particles has a beneficial effect on cell viability. This effect was significantly pronounced for E3-M particles which had the highest cholesterol/escin ratio. As a consequence, these particles had almost negligible effect on cell viability. Significant differences were observed comparing the results after 48 h and 72 h incubation when using CT26.WT cells co-cultured with E16-M particles (100×, 1000×), and with E20-M particles (100×, 1000×).

Next, we prepared new escin nanoparticles based on the E3-M composition, but with higher cholesterol content by adding 31.5 mg cholesterol instead of 22.5 mg to E3 sample. The characteristics of these particles (E3-M2) are shown in Table 2. The additional amount of cholesterol slightly increased the size of the particles without changing their polydispersity. The resulting E3-M2 particles were observed to be hollow, as shown in cryo-TEM micrograph (Fig. 2A). The difference in the contrast between the surface of the particles and their core, indicates well defined surface layer and hollow core, as schematic depicted in Fig. 2C. Therefore, we can expect that different types of antigens can be incorporated inside the particle core or on the particle surface.

The cell viability after incubation with E3-M and E3-M2 particles were tested using A20 and CT26.WT cell lines (Fig. 3). After treatment with modified E3-M2 particles, cells from both lines remained viable, whereas when using E3-M particles at a 10-fold dilution, there were no viable cells after 24 h only.

3.2. Glycyrrhizin particles construction

Following the same experimental protocol as the one used for preparation of E3-M and E3-M2 particles, we prepared new nanoparticles using Glycyrrhizin instead of escin. The properties of particles containing Glycyrrhizin are shown in Table 2. The size and PDI of G3-M particles are very close to those of E3-M particles, whereas much smaller in size particles with low polydispersity were formed

Table 2
Composition of the original and modified samples after cholesterol addition, their absorbance measured before centrifugation and filtration, mean sizes and PDI determined for centrifuged and filtered samples.

	CH post addition	ESC	CH	DPPC	Absorbance	z_{ave}, nm	PDI	d_v, nm	d_I, nm	d_N, nm
E3	No	50	10	40	0.65	93	0.18	83	115	57
E3-M	Yes, once	40.8	26.5	32.7	2.46	122	0.15	118	144	77
E3-M2	Yes, twice	38.0	31.6	30.4	2.62	130	0.15	133	155	87
E16	No	60	10	30	0.59	80	0.15	68	95	50
E16-M	Yes, once	49	26.5	24.5	1.69	105	0.11	95	118	70
E20	No	47.5	5	47.5	0.32	69	0.26	18	91	12
E20-M	Yes, once	38.8	22.4	38.8	2.67	125	0.22	182	196	65
		Glyc	**CH**	**DPPC**	**Absorbance**	**z_{ave}, nm**	**PDI**	**d_v, nm**	**d_I, nm**	**d_N, nm**
G3-M	Yes, once	40.8	26.5	32.7	2.49	130	0.15	133	152	89
G3-M2	Yes, twice	38.0	31.6	30.4	2.63	70	0.11	60	80	50

ESC = escin; CH = cholesterol; DPPC = 1,2-dipalmitoyl-sn-glycero-3-phosphocholine; Glyc = glycyrrhetinic acid; z_{AVE} = intensity based harmonic mean (2,3); PDI = polydispersity index; d_V = mean volume diameter; d_I = mean diameter by intensity; d_N = mean diameter by number.

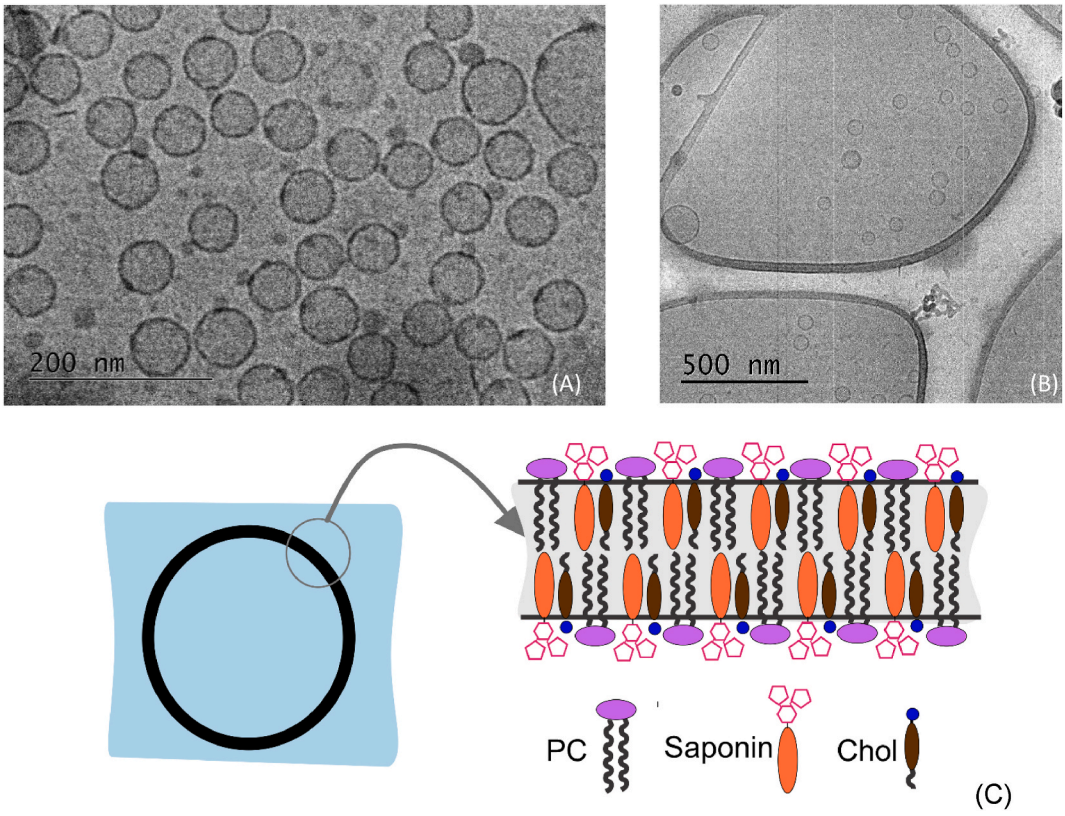

Fig. 2. Cryo-TEM images of the particles from E3-M2 sample, 200 keV, magnification 40000×(A) Without fluorescence dye; (B) after incorporation of Nile red, magnification 10 000×; (C) Schematic presentation of the ISCOM particles formed in the current study. The composition of the bilayer of the formed particles is schematically shown: Saponin = escin; Chol = cholesterol; PC = 1,2-dipalmitoyl-sn-glycero-3-phosphocholine.

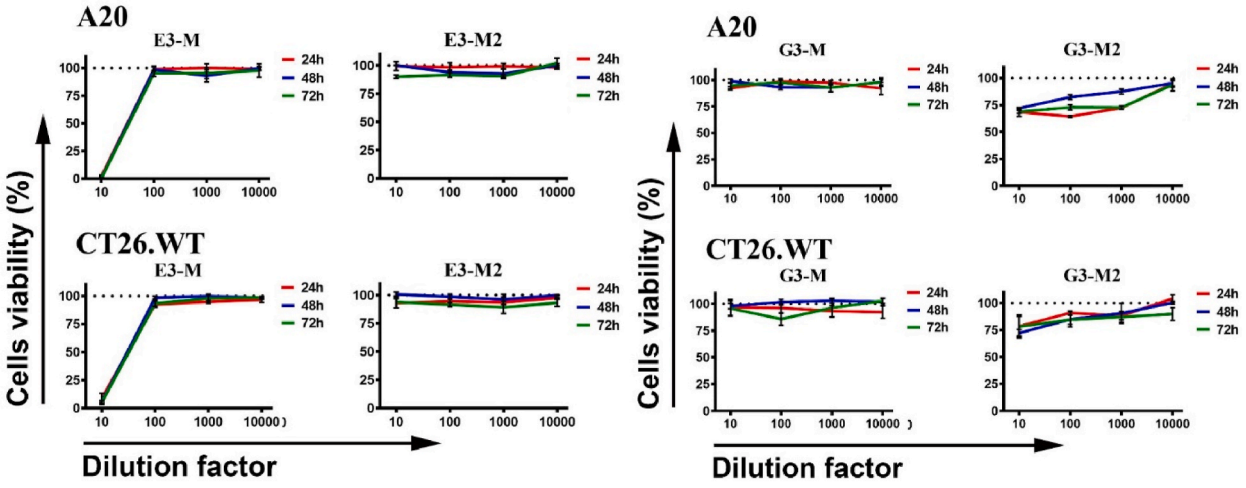

Fig. 3. A20 and CT26.WT cell viability after 24 h (red curves); 48 h (blue curves) and 72 h (green curves) after treatments with modified particles from samples E3-M; E3-M2; G3-M and G3-M2 (from Table 2) as a function of dilution. Untreated cells were used as controls with 100 % viability for each time period. All samples were triplicated and mean ± SD values were presented for each group; p values were calculated using the two-way ANOVA test. A representative of three independent experiments is shown.

after addition of 31.5 mg cholesterol when Glycyrrhizin (instead of escin) was used for particle preparation (cf. G3-M2 and E3-M2).

The toxicity of G3-M and G3-M2 particles was tested on A20 and CT26.WT cells (Fig. 3). Interestingly, better viability was obtained when G3-M particles were used as compared to G3-M2, which is probably related to some structural changes appearing upon further

cholesterol addition. The cholesterol addition also caused a significant decrease in the particle size (see Table 2).

In some additional experiments, the fluorescent dyes Nile Red and Bodipy were included into the particles. The main characteristics of the dye-containing particles are shown in Table 3. Dyes inclusion into the particles has no significant effect on their size and polydispersity.

3.3. Erythrocyte hemolysis assay

Escin-containing particles were utilized in the subsequent experiments due to their stability and low cytotoxicity. This enabled us to continue with the erythrocyte hemolysis experiments. The E3-M2 particles exhibited low levels of erythrocyte hemolysis across all dilution factor, which made them preferable for the next series of experiments (Fig. 4).

3.4. Nanoparticles penetration into the macrophages

FACS analysis was conducted to determine the interaction between the nanoparticles and macrophages. The isolated peritoneal cell population was co-cultured with the 10× diluted nanoparticles E3-M2, incorporated with Nile Red, and further incubated with the macrophage-specific F4/80 antibody. The results from FACS analysis revealed that nearly all of the gated F4/80-positive macrophages had taken the E3-M2- Nile Red nanoparticles (Fig. 5A). It was not possible to use the second included dye, Bodipy, in the same experiment because its spectrum overlaps with the FITC spectrum.

3.5. Fluorescence microscopy analysis

The FACS analysis demonstrated that the nanoparticles were integrated to the F4/80 positive cells. However, further investigation was needed to ascertain whether they were internalized into the cytoplasm or merely attached to the cell surface. For that reason, a fluorescence microscopy analysis was performed. The isolated macrophages were co-cultured with the nanoparticles on microscope slides to verify the particles internalization. The integrity of actin filaments of the cytoskeleton and the nuclear structure were checked as well. The results showed that the Nile Red-containing E3-M2 particles are able to penetrate macrophages and that neither the cytoskeleton, nor the nuclear structure were damaged, Fig. 5B.

4. Discussion

Over the past decade, there has been a significant rise in the utilization of nanoparticles for delivering vaccine components. A variety of nanoparticle types with diverse physicochemical properties, including shape, size, and charge, have been developed for application against viral and bacterial infections. This variety includes gold or iron oxide nanoparticles, polymeric, liposomes, as well as virus-like nanoparticles used as adjuvants or vehicles for pathogen structures delivery. The small size of particles limited to nano-range offers the advantage of scaling to match the size of many viruses or multi-unit proteins, thereby improving cell recognition and internalization [49].

The proposed method for fast formation of safe saponin-cholesterol-phospholipid nanoparticles has been successfully applied to two different saponins, escin and glycerrhizin, yielding similar results and demonstrating its versatility. The particles prepared by this method exhibit a non-perforated structure, resembling liposomes or unilamellar vesicles, as depicted in Fig. 2.

Table 3
Composition of Glycyrrhizin-containing particles after Nile Red or Bodipy inclusion, their absorbance measured before centrifugation and filtration, mean sizes and PDI determined for centrifuged and filtered samples. First fourth rows show the data for particles formed after addition of Nile Red, whereas last fourth rows show the data for particles formed in presence of Bodipy.

	Dye	Absorbance	z_{ave}, nm	PDI	d_v, nm	d_I, nm	d_N, nm
E3-M-N	Nile Red	5.4	130	0.12	133	152	90
	Nile Red	5.7	130	0.12	130	150	85
E3-M2-N							
	Nile Red	4.4	130	0.17	130	155	80
G3-M-N							
	Nile Red	4.3	70	0.10	60	75	45
G3-M2-N							
	Bodipy	5.4	120	0.14	120	140	80
E3-M-B							
	Bodipy	5.3	130	0.11	130	147	90
E3-M2-B							
	Bodipy	4.5	110	0.12	92	120	100
G3-M-B							
	Bodipy	3.3	70	0.10	60	75	46
G3-M2-B							

z_{AVE} = intensity based harmonic mean (2,3); PDI = polydispersity index; d_V = mean volume diameter; d_I = mean diameter by intensity; d_N = mean diameter by number.

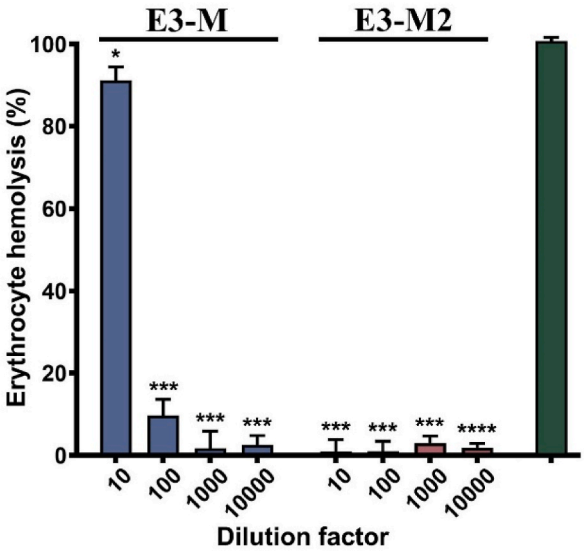

Fig. 4. Erythrocyte hemolysis induced by E3-M and E3-M2 particles as a function of dilution. All samples were triplicated and mean ± SD values were presented for each group; p values were calculated using the two-way ANOVA test (*$p < 0.05$; ***$p < 0.001$; ****$p < 0.0001$) compared to 100 % hemolysis control. A representative of three independent experiments is shown.

The structure of the Escin- and Glycerrhizin-containing particles is different from the structure of the Quillaja-containing ISCOM particles, obtained by the previously established methods; the latter have a cage shape with perforated walls. This difference is attributed to the absence of surfactant in the current method. In the conventional approach, saponins, phospholipid (PC), and cholesterol are first solubilized in a surfactant solution, which is subsequently removed by dialysis. In the newly proposed method, the surfactant is removed, thus leading to solubilization of PC and cholesterol directly into the saponin micelles. The initial mixture reveals various aggregates - micelles, unilamellar vesicles, and cholesterol crystals. The addition of cholesterol enables its incorporation into saponin micelles, facilitating their transformation into unilamellar vesicles with rigid layers during the last cycles of sonication. Subsequent centrifugation and filtration remove the residual DPPC/cholesterol crystals, thus leaving solely the stable vesicles in the aqueous phase. The incorporation of different dyes does not alter the appearance of the particles, as the dyes are initially solubilized in the saponin micelles before being integrated into the final vesicle walls.

These vesicles exhibit the ability to encapsulate water-soluble substances within the vesicles and hydrophobic substances within the hydrophobic vesicle wall. This characteristic will be demonstrated and explored further in a subsequent study, where various peptides are successfully incorporated into the formed particles.

For both saponins used, the safe particles have mean number diameter, $d_N \approx 90$ nm, even after undergoing various stages of cholesterol addition. This consistent diameter suggests that this curvature is characteristic for the vesicle wall. When particle sizes are smaller, cell viability decreases significantly, showing that these particles have flexible bilayers capable of releasing free saponin molecules into the solution. This hypothesis is supported by the presence of elongated particles in these samples (images not shown). Furthermore, the increase of cholesterol content for Glycyrrhizin-particles leads to formation of cholesterol nanoparticles and flexible unilamellar vesicles. As a consequence, free saponin molecules are once again present in the solution, and the corresponding particles (G3-M2) exhibit higher toxicity compared to G3-M1 particles.

The main differences between existing methods and the one proposed in this study are: (1) In the current method instead of using syndet surfactant [1,19,20] for cholesterol and DPPC solubilization, as in the classical method for ISCOM's preparation, saponin micelles are used for cholesterol and DPPC solubilization. (2) To achieve the immobilization of saponin molecules inside the liposomes wall, additional cholesterol is added after particle formation. Otherwise the saponin molecules remain freely exchangeable with the water and the observed hemolytic activity is very high. Previous studies have shown that the inclusion of cholesterol in liposomes increases their rigidity, particle size and incorporation efficiency with respect to retinol [50–53]. However, in the current study, we have shown for the first time that the post-addition of cholesterol to pre-formed liposomes can decrease their hemolytic activity significantly.

The main advantages of the proposed method are: (1) It can be applied to different types of saponins; (2) It can be used for incorporation of water-soluble molecules inside the particle interior and oil-soluble molecules within the particle wall.

The current method relies on the removal of large aggregates through filtration, which can significantly reduce particle yield if larger particles are preferentially formed.

Despite the physical characteristics of nanoparticles, the primary factors determining their application are the purpose for their construction and intended use. Interactions between nanoparticles and targeted cells, followed by cell internalization and interaction with inner membranes and intracellular organelles, can be affected by various factors [54–56]. Weak nanoparticle-cell interaction can result in ineffective cell internalization and delivery, but surface engineering can significantly impact cytotoxic effects. For cytotoxic

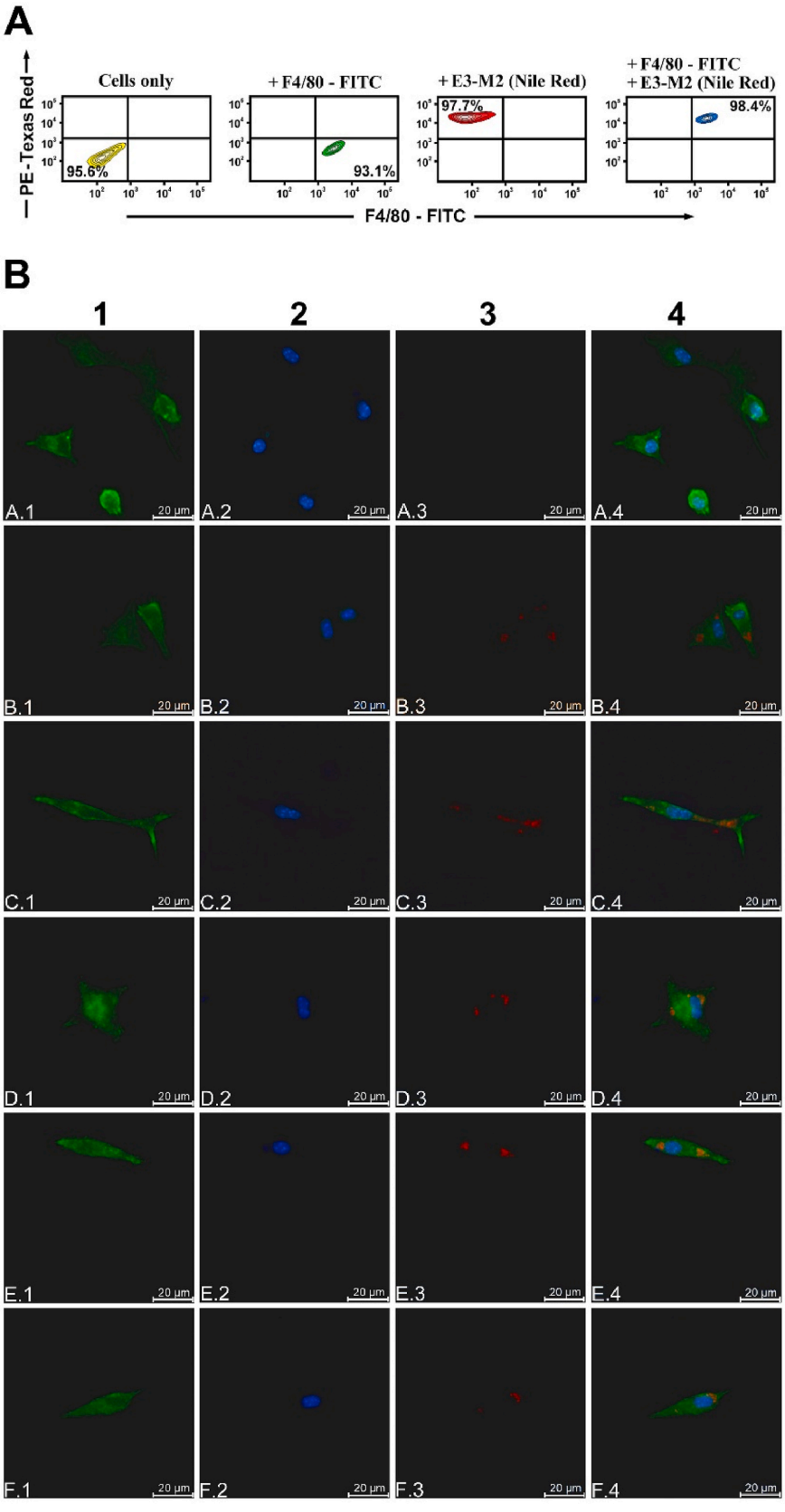

(caption on next page)

Fig. 5. (A) FACS assay for the integration of the E3-M2-Nile Red nanoparticles into the F4/80-positive cells. Isolated mouse macrophages were co-cultured with the nanoparticles E3-M2-Nile Red, and the staining with F4/80-FITC and E3-M2-Nile Red incorporation were measured by flow cytometry. The percentage of stained cells is shown in the quadrants. A representative of four independent experiments is shown. (B) Fluorescence microscopy analysis of the E3-M2-Nile Red included nanoparticles combined with staining of nuclei and actin (bars = 20 μm, magnification 20×). Control cells without E3-M2-Nile Red particles (Line A) validated the protocol and the initial shape of the cells. Experimental slides with E3-M2-Nile Red particles, (Lines B, C, D, E, F) showed the integration of the particles within the cells. Actin Green (Column 1) stained the actin in the cells, while Hoechst stain (Column 2) was used to colour the cells nuclei. The Nile Red E3-M2 included particles (column 3) were observed in the red spectrum. Merged images of all columns are represented in Column 4.

drug delivery in malignant cells therapy and the destruction of pathogenic microorganisms, nanoparticle self-cytotoxicity of can be advantage [43,44]. Conversely, nanoparticles intended for vaccine element delivery must be safe and non-toxic during recognition by mammalian cells and cellular components. Fundamental requirements for these nano-devices carrying viral or bacterial peptides or proteins include high cell viability level during the interactions, absence of nanoparticle-induced hemolysis, and specific penetration into the target cells.

Indeed, following the initial screening of different types of nanoparticles, composed of escin and glycerrhizin based on their effects on cell viability after incubation of all nanoparticles with two cell lines, the selected particles successfully passed the erythrocytes hemolysis test [59–61]. This evaluation was performed within the window between potential cytotoxic concentrations and therapeutic doses. Consequently, the E3-M2 particles were ready for further exploration as potential carriers for specific applications.

The purpose of our experiments is to generate particles such as E3-M2, and to use them for viral peptide carriers in clinical settings. As a logical target for these peptide-loaded nanoparticles we assume the macrophages – important antigen-presenting cells (APCs) during the immune response development after infection or vaccination. These cells express various specific surface receptors involved in the cell activation and adhesion of nanoparticles on cell membranes and subsequent internalization by phagocytosis or by generating temporary pores in the plasma membranes [57,58]. To prove this assumption, we performed FACS analysis to test the Nile Red labeled E3-M2 nanoparticles interaction with isolated mouse macrophages. Indeed, almost 100 % of the F4/80-FITC-gated macrophages were positive for the Nile Red dye, confirming successful interaction between the cells and the E3-M2 nanoparticles. Unfortunately, this experiment cannot answer the question: is the particle just paste to the cell surface after adhesion or it is internalized into the cell. Such complete internalization of nanoparticles can be exhibited by fluorescence microscopy analysis. In our experiments, we observed the internalization of E3-M2 particles, which covers the requirements for their use as a peptide carrier for the next step in developing a new vaccine generation.

Here, we present new nanoparticles which have the potential to be used for the future assembly of a multi-epitope vaccine prototype against SARS-CoV-2, with the aim of being immunogenic in humanized ACE2 transgenic B6.Cg-Tg(K18-ACE2)2Prlmn/J mice. The designed viral epitopes originate from the pool of human SARS-CoV-2 T-cell epitopes, and number of *in vivo* experiments in humanized-ACE2 transgenic mice will exhibit the properties of the generated nanoparticles. This substantial advancement in understanding the interactions between nanoparticles and targeted APCs underscores the need for future research to access the effectiveness of peptide delivery in preclinical trials and animal experiments. Further investigations are required to determine the scalability of the method and to access the *in vivo* efficiency of the prepared nanoparticles containing antigens.

5. Conclusions

In the current study, we developed a new experimental protocol for formation of nanoparticles from PC, cholesterol and two different saponins – escin and glycyrrhetinic acid. The experimental protocol, proposed in the current study, involves the initial formation of nanoparticles through sonication, followed by the addition of cholesterol to the aqueous phase to reduce the concentration of free saponin molecules. Subsequent centrifugation is employed to eliminate aggregates of cholesterol and phospholipids that are not included within the liposomes. This solvent-free method is fast and does not require the use of surfactants.

The formed particles have a mean diameter ranging between 70 and 130 nm, depending on their composition. When cholesterol is post-added to the formed particles, cell viability increases, with 100 % of cells remaining viable even after a 10-fold dilution of the initial particle suspension. The addition of fluorescence dyes (Nile Red and Bodipy) does not significantly affect the shape and size of the prepared particles. Both the MTT viability assay and the erythrocyte hemolysis test identified E3-M2 nanoparticles as safe and suitable for further investigations. E3-M2 particles have demonstrated the ability to deliver molecules such as Nile Red to F4/80-positive cells and can be internalized by macrophages.

CRediT authorship contribution statement

V. Petkov: Visualization, Investigation, Formal analysis. **S. Tsibranska:** Writing – original draft, Visualization, Formal analysis. **I. Manoylov:** Writing – original draft, Methodology, Investigation, Formal analysis. **L. Kechidzhieva:** Visualization, Investigation. **K. Ilieva:** Visualization, Investigation. **S. Bradyanova:** Methodology, Investigation, Formal analysis. **N. Ralchev:** Methodology, Investigation, Formal analysis. **N. Mihaylova:** Methodology, Formal analysis, Conceptualization. **N. Denkov:** Writing – review & editing, Methodology, Conceptualization. **A. Tchorbanov:** Writing – review & editing, Supervision, Methodology, Funding acquisition, Formal analysis, Conceptualization. **S. Tcholakova:** Writing – review & editing, Supervision, Methodology, Formal analysis, Conceptualization.

Ethics statement

This study was reviewed and approved by the Animal Care Commission at the Institute of Microbiology, in accordance with the national regulations.

Data availability statement

Data will be made available on request.

Funding

This work was supported by the Bulgarian Science Fund (Grant No KP-06-DK1/2/2021), and by the Science and Education for Smart Growth Operational Program and co-financed by the European Union through the European Structural and Investment funds (Grants No BG05M2OP001-1.001-0003; BG05M2OP001-1.001-0008 and BG05M2OP001-1.002-0001-C04).

Declaration of competing interest

The authors declare that they have no known competing financial interests or personal relationships that could have appeared to influence the work reported in this paper.

Acknowledgments

We thank Polia Marinova (American College of Sofia, Bulgaria) for the helpful discussions and ideas.

Appendix A. Supplementary data

Supplementary data to this article can be found online at https://doi.org/10.1016/j.heliyon.2025.e41935.

References

[1] B. Morein, B. Sundquist, S. Hoglund, K. Dalsgaard, A. Osterhaus, Iscom, a novel structure for antigenic presentation of membrane proteins from enveloped viruses, Nature 308 (1984) 457–460.
[2] L.J. Peek, C. Russell Middaugh, Cory Berkland, Nanotechnology in vaccine delivery, Adv. Drug Deliv. Rev. 60 (8) (2008) 915–928, https://doi.org/10.1016/j.addr.2007.05.017.
[3] S. Sharma, T. Mukkur, H.A. Benson, Y. Chen, Pharmaceutical aspects of intranasal delivery of vaccines using particulate systems, J. Pharmaceut. Sci. 98 (2009) 812–843.
[4] L. Zhao, A. Seth, N. Wibowo, C.X. Zhao, N. Mitter, C. Yu, A.P. Middelberg, Nanoparticle vaccines, Vaccine 32 (3) (2014) 327–337, https://doi.org/10.1016/j.vaccine.2013.11.069. PMID: 24295808.
[5] M.J. Pearse, D. Drane, ISCOMATRIXTM adjuvant: a potent inducer of humoral and cellular immune responses, Vaccine 22 (2004) 2391–2395.
[6] S. Mohamedi, J. Brewer, J. Alexander, A. Heath, R. Jennings, Antibody responses, cytokine levels and protection of mice immunized with HSV-2 antigens formulated into NISV or ISCOM delivery systems, Vaccine 18 (2000) 2083–2094.
[7] L. Agrawal, W. Haq, C.V. Hanson, D.N. Rao, Generating neutralizing antibodies, Th1 response and MHC non restricted immunogenicity of HIV-I env and gag peptides in liposomes and ISCOMs with in-built adjuvanticity, J. Immune Base Ther. Vaccine 1 (2003) 5–26.
[8] A. Homhuan, S. Prakongpan, P. Poomvises, R.A. Maas, D.J. Crommelin, G.F. Kersten, et al., Virosome and ISCOM vaccines against Newcastle disease: preparation, characterization and immunogenicity, Eur. J. Pharmaceut. Sci. 22 (2004) 459–468.
[9] P.T. Heath, E.P. Galiza, D.N. Baxter, M. Boffito, D. Browne, F. Burns, D.R. Chadwick, R. Clark, C. Cosgrove, J. Galloway, A.L. Goodman, A. Heer, A. Higham, S. Iyengar, A. Jamal, C. Jeanes, P.A. Kalra, C. Kyriakidou, D.F. McAuley, A. Meyrick, A.M. Minassian, J. Minton, P. Moore, I. Munsoor, H. Nicholls, O. Osanlou, J. Packham, C.H. Pretswell, A. San Francisco Ramos, D. Saralaya, R.P. Sheridan, R. Smith, R.L. Soiza, P.A. Swift, E.C. Thomson, J. Turner, M.E. Viljoen, G. Albert, I. Cho, F. Dubovsky, G. Glenn, J. Rivers, A. Robertson, K. Smith, S. Toback, Safety and efficacy of NVX-CoV2373 covid-19 vaccine, N. Engl. J. Med. 385 (2021) 1172–1183.
[10] V. Shinde, S. Bhikha, Z. Hoosain, M. Archary, Q. Bhorat, L. Fairlie, U. Lalloo, M.S.L. Masilela, D. Moodley, S. Hanley, L. Fouche, C. Louw, M. Tameris, N. Singh, A. Goga, K. Dheda, C. Grobbelaar, G. Kruger, N. Carrim-Ganey, V. Baillie, T. de Oliveira, A. Lombard Koen, J.J. Lombaard, R. Mngqibisa, A.E. Bhorat, G. Benadé, N. Lalloo, A. Pitsi, P.-L. Vollgraaff, A. Luabeya, A. Esmail, F.G. Petrick, A. Oommen-Jose, S. Foulkes, K. Ahmed, A. Thombrayil, L. Fries, S. Cloney-Clark, M. Zhu, C. Bennett, G. Albert, E. Faust, J.S. Plested, A. Robertson, S. Neal, I. Cho, G.M. Glenn, F. Dubovsky, S.A. Madhi, Efficacy of NVX-CoV2373 covid-19 vaccine against the B.1.351 variant, N. Engl. J. Med. 384 (2021) 1899–1909.
[11] L.M. Dunkle, K.L. Kotloff, C.L. Gay, G. Áñez, J.M. Adelglass, A.Q. Barrat Hernández, W.L. Harper, D.M. Duncanson, M.A. McArthur, D.F. Florescu, R. S. McClelland, V. Garcia-Fragoso, R.A. Riesenberg, D.B. Musante, D.L. Fried, B.E. Safirstein, M. McKenzie, R.J. Jeanfreau, J.K. Kingsley, J.A. Henderson, D. C. Lane, G.M. Ruíz-Palacios, L. Corey, K.M. Neuzil, R.W. Coombs, A.L. Greninger, J. Hutter, J.A. Ake, K. Smith, W. Woo, I. Cho, G.M. Glenn, F. Dubovsky, Efficacy and safety of NVX-CoV2373 in adults in the United States and Mexico, N. Engl. J. Med. 386 (2022) 531–543.
[12] L. Stertman, Anna-Karin E. Palm, Behdad Zarnegar, Berit Carow, Carolina Lunderius Andersson, Sofia E. Magnusson, Cecilia Carnrot, Vivek Shinde, Gale Smith Gregory Glenn, Louis Fries, Karin Lövgren Bengtsson, The Matrix-M™ adjuvant: a critical component of vaccines for the 21st century, Hum. Vaccines Immunother. 19 (1) (2023) 2189885, https://doi.org/10.1080/21645515.2023.2189885.
[13] K.L. Bengtsson, Bror Morein, Albert DME. Osterhaus, ISCOM technology-based Matrix M™ adjuvant: success in future vaccines relies on formulation, Expert Rev. Vaccines 10 (4) (2011) 401–403, https://doi.org/10.1586/erv.11.25.
[14] K.L. Bengtsson, Haifeng Song, Linda Stertman, Ye Liu, David C. Flyer, Michael J. Massare, Ren-Huan Xu, Bin Zhou, Hanxin Lu, Steve A. Kwilas, Timothy J. Hahn, Eloi Kpamegan, Jay Hooper, Ricardo Carrion Jr., Gregory Glenn, Gale Smith, Matrix-M adjuvant enhances antibody, cellular and protective immune responses of a Zaire Ebola/Makona virus glycoprotein (GP) nanoparticle vaccine in mice, Vaccine 34 (16) (2016) 1927–1935, 7.

[15] S.E. Magnusson, Arwen F. Altenburg, Karin Lövgren Bengtsson, Fons Bosman, Rory D. de Vries, Guus F. Rimmelzwaan, Linda Stertman, Matrix-M™ adjuvant enhances immunogenicity of both protein- and modified vaccinia virus Ankara-based influenza vaccines in mice, Immunol. Res. 66 (2018) 224–233, https://doi.org/10.1007/s12026-018-8991-x.

[16] S. Hoglund, K. Dalsgaard, K. Lovgren, B. Sundquist, A. Osterhaus, B. Morein, ISCOMs and immuno-stimulation with viral antigens, Subcell. Biochem. 15 (1989) 39–68.

[17] H.L. Pham, P.N. Shaw, N.M. Davies, Preparation of immuno-stimulating complexes (ISCOMs) by ether injection, Int. J. Pharm. 310 (2006) 196–202.

[18] K. Lovgren, B. Morein, The requirement of lipids for the formation of immunostimulating complexes (ISCOMs), Biotechnol. Appl. Biochem. 10 (1988) 161–172.

[19] G.F. Kersten, A. Spiekstra, E.C. Beuvery, D.J. Crommelin, On the structure of immune-stimulating saponin-lipid complexes (ISCOMs), Biochim. Biophys. Acta 1062 (2) (1991) 165–171.

[20] G.F. Kersten, D.J. Crommelin, Liposomes and ISCOMs, Vaccine 21 (9– 10) (2003) 915–920.

[21] A. Sjolander, J.C. Cox, I.G. Barr, ISCOMs: an adjuvant with multiple functions, J. Leukoc. Biol. 64 (6) (1998) 713–723.

[22] M. Johansson, K. Lovgreen-Bengtsson, ISCOMs with different quillaja saponin components differ in their immuno-modulating activities, Vaccine 17 (1999) 2894–2900.

[23] D. Da Fonseca, J. Frerichs, M. Singh, H. Snippe, A.F.M. Verheul, Induction of antibody and T-cell responses by immunization with ISCOMs containing the 38-kilodalton protein of mycobacterium tuberculosis, Vaccine 19 (2000) 122–131.

[24] Z. Nazemoroaya, Mohsen Sarafbidabad, Athar Mahdieh, Darya Zeini, Bo Nyström, Use of saponinosomes from Ziziphus spina-christi as anticancer drug carriers, ACS Omega 7 (32) (2022) 28421–28433.

[25] D.G. Lendemans, J. Myschik, S. Hook, T. Rades, Immuno-stimulating complexes prepared by ethanol injection, J. Pharm. Pharmacol. 57 (2005) 729–733.

[26] C.M. Ojiako, Innocent Okoye Ebere, Angus Nnamdi Oli, Chibueze Jeremiah Ike, Charles O. Esimone, Anthony A. Attama, Preliminary studies on the formulation of immune stimulating complexes using saponin from Carica papaya leaves, Heliyon 5 (6) (2019) e01962, https://doi.org/10.1016/j.heliyon.2019.e01962.

[27] M.J. Copland, Rades Thomas, Nigel M. Davies, Hydration of lipid films with an aqueous solution of Quil A: a simple method for the preparation of immune-stimulating complexes, Int. J. Pharm. 196 (2) (2000) 135–139.

[28] C.D. Skene, Philip Sutton. Saponin-adjuvanted particulate vaccines for clinical use, Methods 40 (2006) 53–59.

[29] P.H. Demana, N.M. Davies, B. Berger, U. Vosgerau, T. Rades, J. Myschik, et al., Micron 37 (2006) 724–734.

[30] D. Lombardo, M.A. Kiselev, Methods of liposomes preparation: formation and control factors of versatile nanocarriers for biomedical and nanomedicine application, Pharmaceutics 14 (3) (2022) 543, https://doi.org/10.3390/pharmaceutics14030543.

[31] Y. Yang, L. Wang, M. Yuan, Q. Yu, F. Fu, Anti-inflammatory and gastroprotective effects of escin, Nat. Prod. Commun. 15 (12) (2020), https://doi.org/10.1177/1934578X20982111.

[32] C. de Groot, M. Müsken, C.C. Müller-Goymann, Novel colloidal microstructures of β-escin and the liposomal components cholesterol and DPPC, Planta Med. 84 (16) (2018) 1219–1227, https://doi.org/10.1055/a-0624-2706.

[33] C. Fiore, Michael Eisenhut, Rea Krausse, Eugenio Ragazzi, Donatella Pellati, Decio Armanini, Jens Bielenberg, Antiviral effects of Glycyrrhiza species, Phytother Res. 22 (2008) 141–148.

[34] H. Soufy, Yassein Safaa, Alaa R. Ahmed, Mohamed H. Khodier, Mohamed A. Kutkat, Soad M. Nasr, Faten A. Okda, Antiviral and immune stimulant activities of glycyrrhizin against duck Hepatitis virus, Afr. J. Tradit., Complementary Altern. Med. 9 (3) (2012) 389–395.

[35] L. Zahrei-Abdevand, M. Soltani, Sh Shafiei, Adjuvant effect of Licorice (Glycyrrhiza glabra) extract on the efficacy of lactococcosis vaccine in rainbow trout (Oncorhynchus mykiss), Iran. J. Fish. Sci. 20 (3) (2021) 646–662, https://doi.org/10.22092/ijfs.2021.124006.

[36] H. Chen, Binghe Guan, Bin Wang, Haiwei Pu, Xiaoyu Bai, Xi Chen, Jihong Liu, Caiming Li, Jinhua Qiu, Dan Yang, Kejian Liu, Wang Qi, Suhua Qi, Jiangang Shen, Glycyrrhizin prevents hemorrhagic transformation and improves neurological outcome in ischemic stroke with delayed thrombolysis through targeting peroxynitrite-mediated HMGB1 signaling, Translational Stroke Research 11 (2020) 967–982.

[37] X. Zhao, Yunpeng Fan, Deyun Wang, Yuanliang Hu, Liwei Guo, Shiliang Ruan, Jing Zhang, Yuan Ju, Immunological adjuvant efficacy of glycyrrhetinic acid liposome against Newcastle disease vaccine, Vaccine 29 (2011) 9611–9617.

[38] P. Luo, Dong Liu, Juan Li, Pharmacological perspective: glycyrrhizin may be an efficacious therapeutic agent for COVID-19, Int. J. Antimicrob. Agents 55 (6) (2020) 105995, https://doi.org/10.1016/j.ijantimicag.2020.105995.

[39] C. Bailly, G. Vergoten, Glycyrrhizin: an alternative drug for the treatment of COVID-19 infection and the associated respiratory syndrome? Pharmacol. Ther. 214 (2020) 107618 https://doi.org/10.1016/j.pharmthera.2020.107618. Epub 2020 PMID: 32592716; PMCID: PMC7311916.

[40] S. Banerjee, Sandip Kumar Baidya, Nilanjan Adhikari, Balaram Ghosh, Tarun Jha, Glycyrrhizin as a promising kryptonite against SARS-CoV-2: clinical, experimental, and theoretical evidences, J. Mol. Struct. 1275 (2023) 134642.

[41] R. Augustine, A. Hasan, R. Primavera, R.J. Wilson, A.S. Thakor, B.D. Kevadiya, Cellular uptake and retention of nanoparticles: insights on particle properties and interaction with cellular components, Mater. Today Commun. 25 (2020) 101692.

[42] S. Kahbasi, M. Samadbin, F. Attar, M. Heshmati, D. Danaei, B. Rasti, A. Salihi, N.M.Q. Nanakali, F.M. Aziz, K. Akhtari, A. Hasan, M. Falahati, The effect of aluminum oxide on red blood cell integrity and hemoglobin structure at nanoscale, Int. J. Biol. Macromol. 138 (2019) 800–809, https://doi.org/10.1016/j.ijbiomac.2019.07.154.

[43] B. Le Ouay, F. Stellacci, Antibacterial activity of silver nanoparticles: a surface science insight, Nano Today 10 (2015) 339–354, https://doi.org/10.1016/j.nantod.2015.04.002.

[44] N.A. Gamasaee, H.A. Muhammad, E. Tadayon, M. Ale-Ebrahim, M. Mirpour, M. Sharifi, A. Salihi, M.S. Shekha, A.A.B. Alasady, F.M. Aziz, K. Akhtari, A. Hasan, M. Falahati, The effects of nickel oxide nanoparticles on structural changes, heme degradation, aggregation of hemoglobin and expression of apoptotic genes in lymphocytes, J. Biomol. Struct. Dyn. (2019), https://doi.org/10.1080/07391102.2019.1662850.

[45] K.L. Hess, I.L. Medintz, C.M. Jewell, Designing inorganic nanomaterials for vaccines and immunotherapies, Nano Today 27 (2019) 73–98, https://doi.org/10.1016/j.nantod.2019.04.005.

[46] M. Szwed, M.L. Torgersen, R.V. Kumari, S.K. Yadava, S. Pust, T.G. Iversen, T. Skotland, J. Giri, K. Sandvig, Biological response and cytotoxicity induced by lipid nanocapsules, J. Nanobiotechnol. 18 (1) (2020) 5, https://doi.org/10.1186/s12951-019-0567-y. PMID: 31907052; PMCID: PMC6943936.

[47] E. Winter, C. Dal Pizzol, C. Locatelli, T.B. Crezkynski-Pasa, Development and evaluation of lipid nanoparticles for drug delivery: study of toxicity in, vitro and in vivo, J. Nanosci. Nanotechnol. 16 (2) (2016) 1321–1330, https://doi.org/10.1166/jnn.2016.11667. PMID: 27433582.

[48] S. Mickymaray, M.S. Al Aboody, M.M. Eraqi, W.A. Alhoqail, A.S. Alothaim, K. Suresh, Biopolymer chitosan surface engineering with magnesium oxide-pluronic-F127-escin nanoparticles on human breast carcinoma cell line and microbial strains, Nanomaterials 13 (7) (2023) 1227, https://doi.org/10.3390/nano13071227. PMID: 37049321; PMCID: PMC10097236.

[49] Y. Chan, S.W. Ng, S.K. Singh, M. Gulati, G. Gupta, S.K. Chaudhary, G.B. Hing, T. Collet, R. MacLoughlin, R. Löbenberg, B.G. Oliver, D.K. Chellappan, K. Dua, Revolutionizing polymer-based nanoparticle-linked vaccines for targeting respiratory viruses: a perspective, Life Sci. 280 (2021) 119744, https://doi.org/10.1016/j.lfs.2021.119744. PMID: 34174324; PMCID: PMC8223024.

[50] P. Nakhaei, R. Margiana, D. Bokov, W.K. Abdelbasset, M.A.J. Kouhbanani, R.S. Varma, F. Marofi, M. Jarahian, N. Beheshtkhoo, Liposomes: structure, biomedical applications, and stability parameters with emphasis on cholesterol, Front. Bioeng. Biotechnol. 9 (2021) 705886.

[51] S.-C. Lee, K.-E. Lee, J.-J. Kim, S.-H. Lim, The effect of cholesterol in the liposome bilayer on the stabilization of incorporated retinol, J. Liposome Res. 15 (2005) 157–166.

[52] L. Zhao, F. Temelli, J.M. Curtis, L. Chen, Preparation of liposomes using supercritical carbon dioxide technology: effects of phospholipids and sterols, Food Res. Int. 77 (2015) 63–72, https://doi.org/10.1016/j.foodres.2015.07.006.

[53] S. Kaddah, N. Khreich, F. Kaddah, C. Charcosset, H. Greige-Gerges, Cholesterol modulates the liposome membrane fluidity and permeability for a hydrophilic molecule, Food Chem. Toxicol. 113 (2018) 40–48.

[54] B.D. Kevadiya, B. Ottemann, I.Z. Mukadam, L. Castellanos, et al., Rod-shape theranostic nanoparticles facilitate antiretroviral drug biodistribution and activity in human immunodeficiency virus susceptible cells and tissues, Theranostics 10 (2020) 630–656, https://doi.org/10.7150/thno.39847.

[55] C. Contini, M. Schneemilch, S. Gaisford, N. Quirke, Nanoparticle–membrane interactions, J. Exp. Nanosci. 13 (2018) 62–81, https://doi.org/10.1080/17458080.2017.1413253.
[56] I.Z. Mukadam, J. Machhi, J. Herskovitz, M. Hasan, et al., Rilpivirine-associated aggregation-induced emission enables cell-based nanoparticle tracking, Biomaterials 231 (2020), https://doi.org/10.1016/j.biomaterials.2019.119669.
[57] A. Alexeev, W.E. Uspal, A.C. Balazs, Harnessing Janus nanoparticles to create controllable pores in membranes, ACS Nano 2 (2008) 1117–1122, https://doi.org/10.1021/nn8000998.
[58] J. Lin, A. Alexander-Katz, Cell membranes open "doors" for cationic nanoparticles/biomolecules: insights into uptake kinetics, ACS Nano 7 (2013) 10799–10808, https://doi.org/10.1021/nn4040553.
[59] D.T. Savage, J.Z. Hilt, T.D. Dziubla, In vitro methods for assessing nanoparticle toxicity, Methods Mol. Biol. 1894 (2019) 1–29, https://doi.org/10.1007/978-1-4939-8916-4_1. PMID: 30547452; PMCID: PMC6984383.
[60] V. Kumar, N. Sharma, S.S. Maitra, In vitro and in vivo toxicity assessment of nanoparticles, Int. Nano Lett. 7 (2017) 243–256, https://doi.org/10.1007/s40089-017-0221-3.
[61] J. Lopes, T. Ferreira-Gonçalves, L. Ascensão, A.S. Viana, L. Carvalho, J. Catarino, P. Faísca, A. Oliva, D.P.C. de Barros, C.M.P. Rodrigues, et al., Safety of gold nanoparticles: from in vitro to in vivo testing array checklist, Pharmaceutics 15 (2023) 1120, https://doi.org/10.3390/pharmaceutics15041120.